Revista ALCONPAT
www.revistaalconpat.org
eISSN 2007-6835
Revista de la Asociación Latinoamericana de Control de Calidad, Patología y Recuperación de la Construcción

Reliability-based calibration of fatigue load factors for steel bridges under traffic growth uncertainty.

E. Barragán González [1*]. J. G. Rangel Ramírez[2]
*Contact author: eb@emmanuelbarragan.com
DOI: https://doi.org/10.21041/ra.v16i3.1054

Received: 03/06/2026 | Received in revised form: 09/08/2026 | Accepted: 24/08/2026 | Published: 01/09/2026

ABSTRACT
A reliability-based calibration of the fatigue load factor was performed as a case study for a Mexican steel bridge (Puente Calapa). Empirical Mexican axle-weight distributions gave stresses, processed by rainflow counting, Palmgren-Miner damage accumulation, and Monte Carlo evaluation of a probabilistic limit state. For 2.5%/year growth over 75 years, the Eurocode bilinear S-N curve yielded factors of 1.34 (β=1.0) and 0.70 (β=3.0). The analysis is conditional on a single bridge and idealized structural model. The study's originality lies in making the annual traffic growth rate an explicit calibration input rather than an implicit assumption. Growth rate emerged as the dominant uncertainty, shifting the reliability index by 6.5 units across the examined range and supporting its explicit formulation in code calibration.
Keywords: fatigue; reliability; load factor; traffic growth; steel bridge.

Cite as: Barragán González, E., Rangel Ramírez, J. G. (2026), *"Reliability-based calibration of fatigue load factors for steel bridges under traffic growth uncertainty."*, Revista ALCONPAT, 16 (3), pp. 536 – 557, DOI: https://doi.org/10.21041/ra.v16i3.1054

[1] Tecnologías Sostenibles y Civil, Tecnológico de Monterrey, Campus Puebla.
[2] Profesor, PhD, Tecnologías Sostenibles y Civil, Tecnológico de Monterrey, Campus Puebla.

Contribution of each author
In this work, Author A contributed 50% to experimentation and model development, 100% to data collection, 100% to the writing of the work, and 50% to the discussion of the results; Author B contributed 100% to the original idea, 50% to experimentation and model development, and 50% to the discussion of results.

Discussions and subsequent corrections to the publication
Any dispute, including the replies of the authors, will be published in the second issue of 2027 provided that the information is received before the closing of the second issue of 2027.

Calibración basada en confiabilidad de los factores de carga por fatiga para puentes de acero bajo incertidumbre en el crecimiento del tránsito.

RESUMEN

Se calibró por confiabilidad el factor de carga por fatiga, como estudio de caso, para un puente de acero mexicano. Se calcularon esfuerzos con distribuciones empíricas de peso por eje, conteo Rainflow, daño de Palmgren-Miner y Monte Carlo sobre un estado límite probabilístico. Para 2.5% anual durante 75 años, la curva S-N bilineal del Eurocódigo arrojó factores de 1.34 (β=1.0) y 0.70 (β=3.0). El análisis está condicionado a un solo puente y modelo estructural idealizado. La originalidad radica en tratar el crecimiento del tránsito como dato explícito de calibración y no como suposición implícita. La tasa de crecimiento resultó la principal incertidumbre, desplazando el índice de confiabilidad 6.5 unidades en el rango examinado y respaldando su formulación en futuras calibraciones.

Palabras clave: fatiga; confiabilidad; factor de carga; crecimiento del tráfico; puente de acero.

Calibração baseada em confiabilidade dos fatores de carga de fadiga para pontes de aço sob incerteza de crescimento do tráfego.

RESUMO

Calibrou-se por confiabilidade o fator de carga de fadiga, como estudo de caso, para uma ponte de aço mexicana. Foram calculadas as tensões com distribuições empíricas de peso por eixo, contagem Rainflow, dano de Palmgren-Miner e método de Monte Carlo num estado-limite probabilístico. Para 2.5% ao ano durante 75 anos, a curva S-N bilinear do Eurocódigo apresentou fatores de 1.34 (β=1.0) e 0.70 (β=3.0). A análise limita-se a uma ponte e a um modelo estrutural idealizado. A originalidade reside em tratar o crescimento do tráfego como dado de calibração e não como suposição implícita. A taxa de crescimento revelou-se a principal incerteza, deslocando o índice de confiabilidade em 6.5 unidades no intervalo examinado e respaldando sua formulação em futuras calibrações.

Palavras-chave: fadiga; confiabilidade; fator de carga; crescimento do tráfego; ponte de aço.

Legal Information

Revista ALCONPAT is a quarterly publication by the Asociación Latinoamericana de Control de Calidad, Patología y Recuperación de la Construcción, Internacional, A.C., Km. 6 antigua carretera a Progreso, Mérida, Yucatán, 97310, Tel. +52 1 983 419 8241, alconpat.int@gmail.com, Website: www.alconpat.org

Reservation of rights for exclusive use No.04-2013-011717330300-203, and ISSN 2007-6835, both granted by the Instituto Nacional de Derecho de Autor. Responsible editor: Pedro Castro Borges, Ph.D. Responsible for the last update of this issue, Informatics Unit ALCONPAT, Elizabeth Sabido Maldonado.

The views of the authors do not necessarily reflect the position of the editor.

1. INTRODUCTION

Fatigue is among the principal long-term deterioration mechanisms affecting steel highway bridges, alongside corrosion and corrosion–fatigue interaction, and the calibration of fatigue load factors is correspondingly one of the central tasks of modern bridge code development. Because fatigue damage accumulates irreversibly over the service life of a structure, the load factors adopted at the design stage also govern how the remaining safety margin of an existing bridge is assessed during its operating life and therefore directly relate to inspection planning, service-life estimation, and decisions on intervention.

Both the AASHTO LRFD Bridge Design Specifications (AASHTO, 2024) and the Eurocode (CEN, 2005; CEN, 2006) provide partial safety factors for fatigue verification derived from population-level reliability studies of bridges, weigh-in-motion (WIM) data, and S-N curves. The calibration of AASHTO LRFD strength limit states by Nowak (1999) established the template for this kind of work, and analogous calibrations of the fatigue limit state have since been reported in Moses et al. (1987), Bowman et al. (2012), Berwick (2012), and TRB (2014) for the AASHTO framework and in D'Angelo and Nussbaumer (2017) and Sørensen (2012) for the Eurocode framework.

A common feature of these calibrations is that the assumed long-term traffic pattern is fixed when the load factors are derived. The forecast traffic growth rate enters the calibration implicitly, through the choice of design vehicle and the assumed lifetime accumulation. Once embedded in the factors, the underlying growth assumption is no longer adjustable by the engineer at the design stage: a 2%/year growth scenario and a 5%/year growth scenario, applied to the same bridge over a 75-year horizon, lead to substantially different accumulated fatigue damage, but the AASHTO Fatigue I load factor of 1.75 (or Fatigue II of 0.80) is the same in both cases. In environments where the actual heavy-traffic growth rate departs substantially from the implicit assumptions of the codes, this may introduce unquantified bias in the calibrated reliability at the design life.

Mexico is one such environment. Historical annual growth rates of cumulative truck traffic along major Mexican fee highways have been reported in the 2.5 to 3.0 percent per year range; this value is also broadly consistent with the upper end of the global range quoted in the National Cooperative Highway Research Program (NCHRP) Report 299 (Moses et al., 1987).

Mexican legal vehicle configurations, established by NOM-012-SCT-2 (DOF, 2017), also depart substantially from the AASHTO design vehicles against which the codes were calibrated: the heaviest legal Mexican configuration (T3-S2-R4, nine axles) has a base gross-vehicle-weight limit of 66.5 t (~652.1 kN), extended to 75.5 t (~740.4 kN) with the allowance for air-suspension and safety systems, corresponding to approximately 2.28 times the AASHTO HS20-44 design vehicle (325 kN, 33 t). Field weigh-in-motion data from the Instituto Mexicano del Transporte (IMT, 2016) show that approximately one quarter of T3-S2-R4 vehicles exceed even the Mexican legal limit, with observed peak values reaching 92.4 t (~906 kN), or 1.22 times the legal maximum.

The disconnect between the loadings against which existing codes were calibrated and those actually observed on Mexican infrastructure motivates the Mexico-specific reliability-based calibration of fatigue factors, as previously argued by Avendaño et al. (2013) and García-Soto et al. (2015).

The consequences of this disconnect are not confined to new design. A substantial portion of the existing Mexican federal highway bridges were built in the 1990s or earlier, under load models that did not anticipate present-day traffic volumes or configurations, and these structures are now being operated well into their assumed service lives. For such structures, the practical question is not which factor to adopt for a new design, but how much of the assumed fatigue margin has already been consumed and how quickly the remainder is being expended under observed traffic. A calibration that makes the assumed growth rate an explicit input addresses this question directly.

The present study is therefore framed as a case study of an in-service structure rather than as a design exercise.
The present study contributes to this line of work in one specific way: it makes the assumed traffic growth rate an explicit input to the calibration and reports the calibrated load factor as a function of that input. The methodology combines empirical Mexican traffic data with a probabilistic fatigue limit state in the form proposed by Kwon and Frangopol (2010) and systematized by D'Angelo and Nussbaumer (2017), applied to a specific case-study bridge (Puente Calapa, on the Cuacnopalan-Oaxaca fee highway) for which empirical axle-weight distributions and traffic counts are available from public Mexican government sources. The output is a set of calibrated load factors, indexed by the assumed annual growth rate, that exposes the influence of this single input on the calibrated reliability at the analysis period. Puente Calapa has been in service since 1995 and is reported as operational, which allows the calibrated factors to be interpreted against an observed absence of fatigue distress (section 8.5) rather than against a purely hypothetical structure.
The remainder of the paper is structured as follows. Section 2 describes the case-study bridge, the traffic data sources, and the probabilistic vehicle modeling, and develops the structural model, adopting a continuous-span correction to approximate the real five-span continuous geometry as an effective single-span analysis. Section 3 introduces the cycle counting, S-N curves, Palmgren-Miner damage accumulation, and the probabilistic limit-state function. Section 4 develops the exponential traffic-growth model and the closed-form damage trajectory. Sections 5 and 6 describe the Monte Carlo reliability evaluation and the calibration procedure, including the two reliability targets (β_{target} = 1.0 and β_{target} = 3.0) used to bracket the AASHTO and Eurocode conventions respectively. Section 7 reports the calibration outputs at the baseline scenario, the dependence of the calibrated factor on the assumed growth rate, and the sensitivity of the reliability index at the design horizon to growth. Section 8 discusses the interpretation of the calibrated factors, the divergence between the Eurocode and AASHTO S-N conventions observed for this spectrum, the comparison between Mexican and design loadings, and the dominance of growth-rate uncertainty over the other modeling assumptions, as well as the limitations of the study. Section 9 collects the principal findings and points to the possible extension toward a population-level calibration with explicit growth-rate formulation.

2. TRAFFIC AND STRUCTURAL MODELING

The fatigue analysis combines a Mexican traffic loading representation, an empirical axle-weight characterization based on weigh-in-motion data, and a structural model for the case-study bridge.

2.1 Case study: Puente Calapa

The case-study structure is Puente Calapa, a multi-span steel bridge on the Cuacnopalan-Oaxaca fee highway (km 70.7), in central Mexico (see Figure 1).

Figure 1. Case-study bridge Puente Calapa. (a) Bridge overview, from Suarez, 2025 (b) Location on the Cuacnopalan–Oaxaca fee highway, central Mexico. Obtained with Google Earth.

The superstructure is composite (*superestructura mixta*) and consists of five continuous spans of either 75.6 or 57.6 m, supported on common steel girders. The bridge has been in service since 1995. Detailed structural drawings were not available; the geometric properties used in this analysis were estimated by Meneses Rojas (2026) by scaling representative steel girder dimensions (Figure 2). These properties are second moment of area $I = 0.1089\, m^4$, cross-sectional area $A = 0.1637\, m^2$, and centroid distance $y = 1.0\, m$ for one of the two main steel girders described in the same source. Likewise, A572 Gr. 50 steel is assumed.

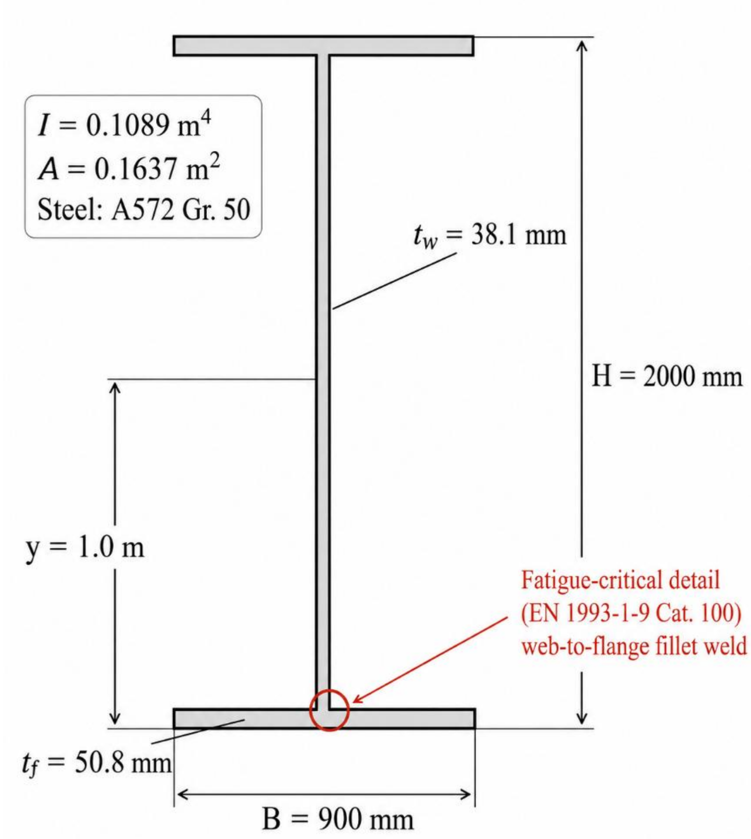

Figure 2. Analyzed girder cross-section

The analysis adopts the bare steel section properties and idealizes a single girder simply supported over a span $L = 76.5\ m$, approximating one of the central spans of the actual continuous structure. A correction factor for continuous-span behavior is introduced in section 2.4 to compensate for the simplification.

2.2 Traffic data and vehicle class statistics.

Traffic loading is characterized by using two complementary public data sources for the case-study site. The Secretaría de Infraestructura, Comunicaciones y Transportes *Datos Viales* dataset (SCT, n.d.) provides the average daily traffic (TDPA, *tránsito diario promedio anual*) and its breakdown by vehicle class. The TDPA reported by SCT is bidirectional; since each girder of the bridge carries traffic in only one direction, the per-girder loading rate is taken as half of the reported value. Using the historical 1995 baseline, corresponding to the bridge's opening year, yields a per-girder rate of 2,772 vehicles per day. Because each girder is loaded by a single traffic lane, no multi-lane reduction or amplification is applied.

The vehicle class distribution at the same station is dominated by passenger vehicles, with heavy multi-axle freight configurations representing a small but disproportionately damaging fraction of the traffic stream. The class probabilities used in the simulation, expressed as percentages of the daily total, are 0.9% motorcycles, 69.2% passenger cars, 6.4% buses, 4.9% C2, 6.4% C3, 5.9% T3-S2, 1.7% T3-S3, 3.7% T3-S2-R4, and 0.9% other configurations, following the breakdown reported by Meneses Rojas (2026).

2.3 Probabilistic vehicle and axle load modeling.

Each simulated vehicle is represented as a sequence of axles with class-specific count, inter-axle spacings, and per-axle weight distributions. Inter-axle spacings are taken as deterministic, set to standard configuration values consistent with the legal definitions of NOM-012-SCT-2 (DOF, 2017).

Per-axle weights for the heavy freight classes (C2, C3, T3-S2, T3-S3, and T3-S2-R4) are drawn from empirical distributions reported in the Instituto Mexicano del Transporte's *Estudio Estadístico de Campo del Autotransporte Nacional* (IMT, 2016), station PC Tehuacán, which contains 16,165 individual vehicle records. For each class, a normal distribution is fitted to the per-axle empirical mean and standard deviation, with axle weights sampled independently. Two findings from this data set have an immediate impact on the characterization of loading. First, the heaviest legal Mexican configuration (T3-S2-R4) has nine axles. Second, and most importantly, of the 704 weighed T3-S2-R4 vehicles in the dataset, approximately 24% exceed the 75.5 t legal gross-vehicle-weight limit established in NOM-012-SCT-2, with the maximum observation reaching 92.4 t (1.22 times the legal limit). This overloading factor is a feature of the present loading conditions that any fatigue analysis specific to Mexican infrastructure should likely incorporate.

Passenger vehicles, motorcycles, and buses are not weighed in the IMT campaign and are represented by normally distributed fallbacks based on typical weight assumptions for each class. These classes individually contribute negligible damage. A passenger car produces stress ranges on the order of 1.5 MPa, compared with peak ranges exceeding 60 MPa for the heaviest configurations.

Vehicle crossings are simulated sequentially, and arrival times are not modeled explicitly. This treatment is appropriate for the present analysis because Palmgren-Miner accumulation is order-independent, so the sequence in which crossings occur does not affect the accumulated damage, and because the single-lane-per-direction geometry of the case-study bridge prevents two heavy vehicles from simultaneously loading the midspan region (see section 2.4). The arrival process therefore does not influence the stress-range spectrum obtained from the simulation.

2.4 Structural model and midspan bending moment calculation.

The midspan bending moment time history for each vehicle passage is obtained by classical beam theory. The girder is idealized as simply supported with span $L = 76.5\,m$, and the vehicle is moved longitudinally in small increments. At each position, only axles located on the bridge contribute; support reactions are computed from static equilibrium, and the midspan moment is obtained from left-section equilibrium analysis. The output is a discrete time series of midspan bending moment $M(t)$ for each crossing.

The simply-supported idealization overestimates midspan moments compared to the actual continuous-girder behavior of Puente Calapa. Johnson et al. (2020) compared simply supported and three-span continuous bridges of common 75-foot spans under moving loads and reported that the maximum equivalent moment at midspan of a continuous span is consistently lower than that of the simply supported reference, with reductions on the order of 25% to 35%. To approximately incorporate this effect without explicit influence-line analysis of the five-span continuous structure, a constant moment correction factor is applied (Equation 1) with $k = 0.7$ for all simulations reported below.

$$M_{midspan}^{corrected}(t) = k \cdot M_{midspan}(t) \tag{1}$$

This is a conservative midpoint of the range reported by Johnson et al. (2020) and represents the principal modeling simplification of the structural analysis. A similar correction was performed for the dead load moment too.

Puente Calapa carries one traffic lane per direction, with each girder loaded by traffic in only one direction; the per-girder loading rate adopted in section 2.2 reflects this configuration. Under this arrangement, heavy vehicles in the same lane are constrained by the minimum safe headway distance and cannot physically produce a two-vehicle span load within legal driving conditions. Simultaneous vehicle presence in opposite directions transfers only partially to the analyzed girder through the deck slab, and we conservatively assume (as stated in section 2.2) that each girder carries the entirety of its lane's load instead of distributing it to the other girder. Explicit modeling of multi-vehicle presence is left as a possible extension for a population-level calibration in which multi-lane bridges are represented.

Finally, a dynamic load factor was not applied to the simulated moment histories. The dynamic amplification of bridge response to moving vehicles is governed by the relationship between the loading frequency and the structure's fundamental frequency, and is most pronounced for short, stiff spans. For the 76.5 m span analyzed here, the vehicle crossing time at highway speed is on the order of three seconds, corresponding to a loading event well below the fundamental frequency expected of a span of this length. Therefore, the response is close to quasi-static.

Any dynamic residual contribution not captured by the quasi-static treatment would increase the simulated stress ranges, and the calibrated load factors reported here are correspondingly non-conservative. This is noted as a limitation in section 8.6.

2.5 Stress calculation.

The corrected bending moment time history is converted to stress at the fatigue-critical location (midspan, bottom flange) by the elastic relation given in Equation 2, where $y = 1.0\,m$ is the distance from the section centroid to the bottom fiber.

$$\sigma_b(t) = \frac{M_{midspan}^{corrected}(t) \cdot y}{I} \tag{2}$$

The dead-load stress at the analyzed cross-section, computed from the steel self-weight and a deck contribution per girder, is 187 MPa. This value is reported here for context on the section properties; under the range-only S-N convention adopted in section 3.2, the dead-load stress does not enter the fatigue limit-state function.

2.6 Summary of stochastic simulation procedure.

The traffic simulation proceeds as follows. For each of the 1,011,780 vehicle crossings comprising one year at the reference TDPA, a vehicle class is drawn from the categorical distribution of class probabilities given in section 2.2. Conditional on the class, the number of axles and the inter-axle spacings are assigned deterministically from the configuration definitions of NOM-012-SCT-2-2017 (section 2.3), and each axle weight is drawn independently from a normal distribution fitted to the per-axle mean and standard deviation reported for that class in the IMT (2016) field campaign at Station PC Tehuacán, which comprises 16,165 weighed vehicle records. Vehicles with a total weight below 200 kgf (1.96 kN) are excluded from the damage accounting as they produce negligible stress ranges.

The stochastic elements of the traffic simulation are therefore the vehicle class and the individual axle weights. All other quantities entering the moment calculation (span length, section properties, inter-axle spacings, continuity correction) are deterministic. The traffic growth rate is treated as a deterministic scenario parameter and swept across the range given in section 4.3, rather than assigned a distribution.

Two further random variables exist, but at the reliability stage rather than the traffic stage: the critical Miner damage at failure Δ, and the modeling-uncertainty factor e, both lognormal, as described in section 3.4. These are sampled $N = 5 \times 10^5$ times per independent evaluation of the limit state, using Monte Carlo as described in section 5.1.

Direct validation of the simulated stress spectrum against field measurement was not possible, as no instrumented monitoring data are available for the case-study structure. Two consistency checks were applied instead. First, the computed dead-load stress at the analyzed section agrees with the value independently reported for the same structure by Meneses Rojas (2026). Second, the nominal fatigue life obtained at constant traffic is consistent with the continued service of the bridge since 1995 without reported fatigue distress (section 8.5). Validation against measured strain histories would be a natural next step and is noted as a limitation in section 8.6.

3. PROBABILISTIC FATIGUE MODEL

The fatigue reliability assessment combines a cycle-counting algorithm applied to the simulated stress histories, an S-N curve, the Palmgren-Miner damage accumulation rule, and a probabilistic limit-state function that captures the uncertainty in fatigue resistance.

3.1 Cycle counting and stress range representation.

Rainflow cycle counting per the ASTM E1049-85 four-point algorithm (ASTM, 2017; Matsuishi and Endo, 1968) resolves each simulated stress history into a list of closed cycles, each described by a range $\Delta\sigma_i$, a mean stress $\sigma_{m,i}$, and a count n_i (1.0 for full cycles closed and 0.5 for residual half-cycles).

For the 76.5 m span analyzed here, the axle group of even the longest legal Mexican configuration occupies approximately one-quarter of the span, and the resulting midspan influence line produces a single smooth loading and unloading event per crossing; the rainflow counting algorithm accordingly resolves each vehicle passage into a single counted cycle. The algorithm is retained rather than replaced by a simple peak-to-valley range because it is the standard treatment for variable-amplitude histories and because the sub-cycle structure it captures would become

significant for shorter spans, where the vehicle length is comparable to the span.
Figure 3 shows the simulated stress history for a single representative T3-S2-R4 crossing. The smooth, single-peaked shape reflects the vehicle's passage across the span, with the nine axles acting as an effectively concentrated load over the influence line of the analyzed section.

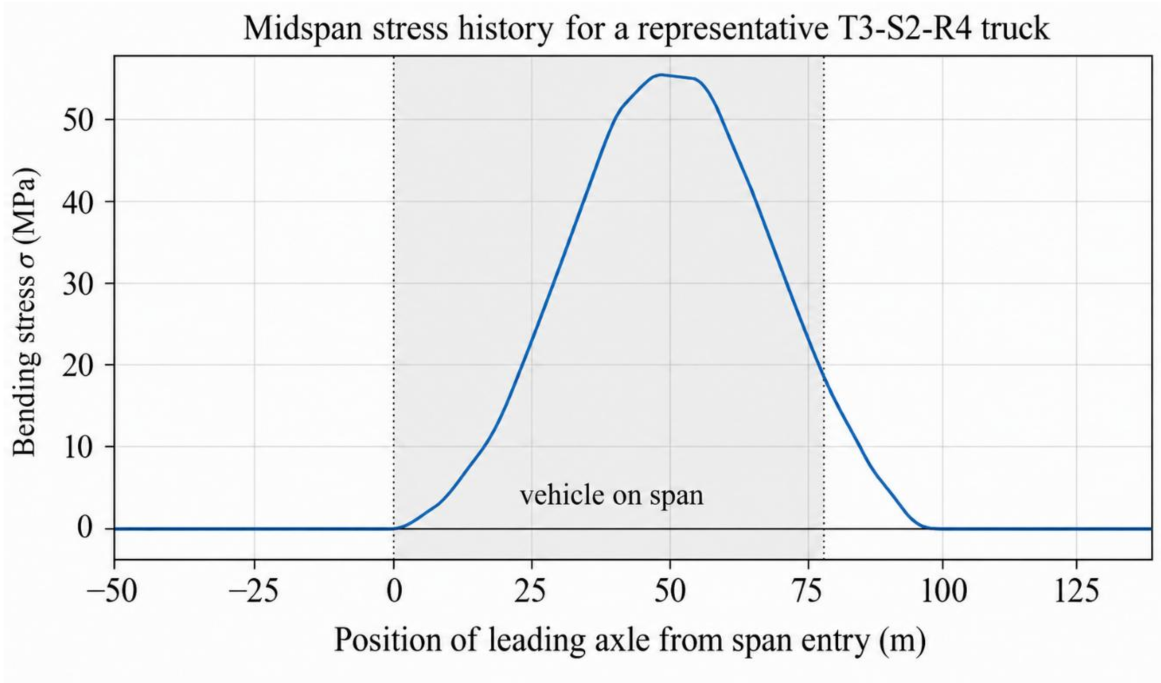

Figure 3. Simulated midspan bending stress history for a representative T3-S2-R4 crossing.

3.2 S-N curve

Fatigue strength is represented by the bilinear S-N curve of Eurocode 3 Part 1-9 (CEN, 2005) of Equation 3:

$$N(\Delta\sigma) = \begin{cases} N_C \cdot \left(\frac{\Delta\sigma_C}{\Delta\sigma}\right)^{m_1} & for\ \Delta\sigma \geq \Delta\sigma_D \\ N_D \cdot \left(\frac{\Delta\sigma_D}{\Delta\sigma}\right)^{m_2} & for\ \Delta\sigma_L \leq \Delta\sigma < \Delta\sigma_D \\ \infty & for\ \Delta\sigma < \Delta\sigma_L \end{cases} \quad (3)$$

where $\Delta\sigma_C$ is the detail-category fatigue strength at $N_C = 2 \times 10^6\ cycles$, $\Delta\sigma_D = \Delta\sigma_C \cdot (N_C/N_D)^{1/m_1}$ is the constant-amplitude fatigue limit (CAFL) at $N_D = 5 \times 10^6$ cycles, and $\Delta\sigma_L = \Delta\sigma_D \cdot (N_D/N_L)^{1/m_2}$ is the cut-off limit at $N_L = 10^8$ cycles. The slope of the S-N curve is $m_1 = 3$ above the CAFL and $m_2 = 5$ below it.

In the absence of detailed information on the controlling fatigue detail at the midspan, EN 1993-1-9 detail category $\Delta\sigma_C = 100\ MPa$ is adopted, corresponding to a continuous longitudinal fillet weld between the web and the bottom flange of a built-up plate girder. The sensitivity of the calibrated load factor to this assumption is discussed in section 8.6.

The single-slope S-N curve of AASHTO LRFD (AASHTO, 2024), in which $m = 3$ for all detail categories and stress ranges below the constant-amplitude fatigue threshold contribute zero damage, is also computed for comparison. The two formulations agree above the CAFL but differ in the sub-CAFL regime, where the Eurocode m=5 branch continues to accumulate damage and AASHTO does not. This distinction is examined quantitatively in the results.

3.3 Cumulative damage.

Fatigue damage is accumulated linearly using Palmgren-Miner's rule (Miner, 1945) of Equation 4:

$$D = \sum_i \frac{n_i}{N_i(\Delta\sigma_i)} \tag{4}$$

where n_i and $\Delta\sigma_i$ are the cycle count and range from rainflow analysis, and N_i is the cycles to failure from Equation (3). Cycles below the cut-off limit $\Delta\sigma_L$ contribute zero damage. The annual damage D_{base} is obtained by simulating the amount TDPA over an entire year.

3.4 Probabilistic modeling of uncertainty.

Two random variables enter the limit state. First, the critical Miner damage at failure Δ accounts for the stochastic nature of fatigue and the well-documented deviation of the empirical Miner sum at failure from unity. Following Wirsching (1984), who established the lognormal fit through statistical analysis of a large body of experimental fatigue test data on welded steel details, Δ is modeled as a lognormal variable with mean $\mu_\Delta = 1.0$ and coefficient of variation $COV_\Delta = 0.30$. This distributional choice has been adopted as the reference prior in the JCSS (Joint Committee on Structural Safety) Probabilistic Model Code Part 3.12 (JCSS, 2011). Second, a single multiplicative modeling-uncertainty factor, e, on the load side captures the combined contributions of load-effect uncertainty, stress concentration, and S-N model uncertainty. Following the formulation of Kwon and Frangopol (2010), e is modeled as lognormal with $\mu_e = 1.0$ and $COV_e = 0.15$.

The traffic growth rate $\alpha_{traffic}$ is treated as a deterministic input parameter, swept across a range of plausible values to establish the sensitivity of the calibrated load factor to assumed growth.

3.5 Limit-state function.

The fatigue limit state for the design horizon t is given by Equation 5:

$$g(t) = \Delta - e \cdot x_F \cdot D_{grown}(t) \tag{5}$$

where x_F is the deterministic load factor under calibration and $D_{grown}(t)$ is the cumulative Miner damage accumulated through year t, including the effect of traffic growth (defined formally in section 4). Failure occurs whenever $g(t) < 0$.

Each Monte Carlo iteration therefore consists of one independent draw of (Δ, e) from their respective lognormal priors, with the deterministic quantities x_F and $D_{grown}(t)$ held fixed.

The structure of Equation (5) follows directly from Equation 10 of Kwon and Frangopol (2010), with two adaptations: the deterministic load factor x_F is introduced, and the damage term is time-evolved to capture exponential traffic growth over the design horizon. Within the categorization of Eurocode partial-factor calibration proposed by D'Angelo and Nussbaumer (2017), this corresponds to "Verification Scheme 3" (damage accumulation).

4. TRAFFIC GROWTH MODELING

The fatigue calibration of section 6 is parameterized by a single deterministic assumed annual rate of growth of traffic. This section formalizes the growth model and derives the expression for the damage trajectory.

4.1 Exponential growth and the literature context.
Long-term traffic forecasting commonly uses an exponential growth model in which the daily traffic at year t relates to the reference-year value by $V(t) = V_0 \cdot (1 + \alpha_{traffic})^t$, where $\alpha_{traffic}$ is the annual growth rate and V is the daily average traffic volume. The exponential form is recommended for fatigue evaluation by NCHRP Report 299, which observes that "traffic volumes usually grow at an annual rate of about 3 to 5 percent until they reach a very high limiting value" (Moses et al., 1987). More recent calibration work continues to adopt the same form: Zhang et al. (2024) formulate long-term fatigue reliability as a function of an exponential traffic growth coefficient.
The exponential model is conservative for very long horizons because it omits saturation effects (Moses et al., 1987); over the 75-year design horizon adopted here, however, the exponential form is the standard choice and is retained throughout this analysis.

4.2 Cumulative damage under exponential growth.
If D_{base} is the annual Miner damage at the reference daily average traffic volume (assumed stationary within a calendar year), and traffic grows exponentially, then the damage accumulated through year t is obtained by Equation 6:

$$D_{grown}(t) = D_{base} \sum_{k=1}^{t} (1 + \alpha_{traffic})^k \qquad (6)$$

For the limiting case $\alpha_{traffic} = 0$, Equation (6) reduces to $D_{grown}(t) = D_{base} \cdot t$, the flat-traffic accumulation. The ratio $D_{grown}(T)/(D_{base} \cdot T)$ quantifies the effect of growth on the damage at the design horizon: for $T = 75$ years and central Mexican growth rates of 2–3% per year, the multiplier is approximately 2.6 to 3.5 relative to static traffic.

4.3 Calibration as a function of growth.
The substitution of Equation (6) into the limit-state function $g(t) = \Delta - e \cdot x_F \cdot D_{grown}(t)$ converts $\alpha_{traffic}$ into a deterministic input parameter of the reliability analysis. For each combination of ($\alpha_{traffic}$, β_{target}, S-N convention), the calibration procedure of section 6 yields a distinct calibrated load factor x_F. The calibration is therefore performed not at a single nominal growth rate, but across a range of plausible scenarios to map the dependence $x_F = x_F(\alpha_{traffic})$ explicitly.
The growth rate range used in the sensitivity analysis is $\alpha_{traffic} \in \{0.5, 1.0, 2.0, 2.5, 3.0, 4.0, 5.0\}$ %/year. The range extends below the historical Mexican observations to include low-growth scenarios and above it to the upper end of NCHRP 299's quoted band.

5. MONTE CARLO RELIABILITY ANALYSIS

The time-dependent probability of fatigue failure is evaluated by direct Monte Carlo simulation of the limit-state function defined in Equation (5).

5.1 Sampling.
For each evaluation of $g(t)$, N independent realizations of the random variables Δ and e are drawn from their respective lognormal distributions. The deterministic load factor x_F and the deterministic damage trajectory $D_{grown}(t)$ enter as fixed values for that evaluation. Throughout this study, $N = 5 \times 10^5$ samples are used per (t, x_F) point.

5.2 Probability of failure and reliability index.
The probability of failure at time t is given by Equation 7:

$$P_f(t) = P(g(t) < 0), \quad (7)$$

estimated within the Monte Carlo framework as the failure fraction, obtained through Equation 8:

$$P_f(t) \approx \frac{1}{N}\sum_{j=1}^{N} \mathbb{1}(g_j(t) < 0), \quad (8)$$

where $\mathbb{1}(\cdot)$ is the indicator function. Finally, the reliability index is then obtained directly from P_f, as seen in Equation 9:

$$\beta(t) = -\Phi^{-1}(P_f(t)), \quad (9)$$

where Φ^{-1} is the inverse standard normal cumulative distribution function.

5.3 Time-dependent failure probability.
Because $D_{grown}(t)$ is strictly increasing in t, $P_f(t)$ is also increasing, and $\beta(t)$ is therefore decreasing for any fixed x_F. The full $\beta(t)$ trajectory is obtained by evaluating $g(t)$ on a discrete grid of years from $t = 1$ to $t = T_{design} + 25$, with the design horizon T_{design} marked explicitly on all reported curves. The time-dependent reliability profile is the basis for the calibration procedure of section 6.

6. CALIBRATION OF LOAD FACTOR

The fatigue load factor x_F is calibrated so that the reliability index at the design period meets a prescribed target.

6.1 Target reliability.
Two target reliability indices are considered, reflecting the two principal conventions used in fatigue code calibration:

- $\beta_{target} = 1.0$, consistent with the AASHTO LRFD fatigue limit state. Earlier work by Berwick (2012) estimated the implicit reliability of the pre-SHRP2 (the second Strategic Highway Research Program) AASHTO Fatigue I limit state at $P_f \approx 0.025$ (equivalent to $\beta \approx 2.0$), but the operative target adopted in the SHRP2 R19B recalibration that produced the current Fatigue I and Fatigue II load factors was $\beta = 1.0$, applied uniformly to both

steel and concrete fatigue elements (TRB, 2014; Bowman et al., 2012). This value is adopted here for the AASHTO-aligned case.
- $\beta_{target} = 3.0$, consistent with Eurocode practice for fatigue-critical welded steel details. D'Angelo and Nussbaumer (2017) derive this value using target reliability indexes recommended from the JCSS: $\beta_{target} = -\Phi^{-1}[\Phi(4.2)]^{100} = 3.0$ for a 100-year reference period and adopt it as the target for Eurocode-aligned fatigue calibration.

Reporting the calibration under both targets makes the results comparable to either an AASHTO-aligned or a Eurocode-aligned regulatory framework. The target probabilities of failure are given by Equation 10:

$$P_{f,target} = \Phi(-\beta_{target}) \tag{10}$$

yielding $P_{f,target} = 0.159$ for $\beta_{target} = 1.0$ and $P_{f,target} = 1.35 \times 10^{-3}$ for $\beta_{target} = 3.0$.

6.2 Design horizon

The design horizon is taken as $T_{design} = 75\ years$, consistent with the standard AASHTO LRFD bridge service-life assumption (AASHTO, 2024). This horizon is used for both the calibration target and all reported sensitivity analyses.

6.3 Calibration procedure

For each combination of β_{target} and traffic growth rate $\alpha_{traffic}$, the calibration proceeds as follows. A grid of trial load factors $x_F \in [0.05, 4.0]$ is constructed. The upper bound was set at 4.0 because the Eurocode calibration (the primary calibration of interest) falls comfortably within this range at both reliability targets. For each candidate, the cumulative damage trajectory $D_{grown}(t)$ is computed, and the Monte Carlo procedure of section 5 is used to evaluate $\beta(T_{design})$. The result is a set of $(x_F, \beta(T_{design}))$.

The calibrated load factor x_F is then defined as the value satisfying Equation 11:

$$\beta(T_{design};\, x_F) = \beta_{target} \tag{11}$$

The calibrated value is obtained by linear interpolation of the computed pairs. This procedure is repeated independently for each S-N convention (Eurocode and AASHTO), each β_{target}, and each scenario value of $\alpha_{traffic}$, producing the calibration curves reported in the results.

6.4 Interpretation of the calibrated factor

A calibrated value $x_F > 1$ indicates that the simulated loading produces a reliability index above the target at the design horizon, and that the structure could in principle carry x_F times the simulated loading before reliability falls precisely to the target. The factor in this case represents the multiplicative safety margin against the chosen target.

A calibrated value $x_F < 1$ indicates that the simulated loading produces a reliability index beneath the target. The factor in this case represents the fraction of the simulated loading at which the target is just met. Equivalently, the loading would need to be reduced by a factor of $1 - x_F$ to bring the reliability to the target.

This dual interpretation is consequential for the case-study results: the unfactored loading at $x_F = 1$ produces a reliability between the two adopted targets, exceeding the AASHTO-aligned $\beta_{target} = 1.0$ but falling short of the Eurocode-aligned $\beta_{target} = 3.0$. The two calibrated factors therefore have opposite signs of deviation from unity, reflecting the fact that the bridge meets one target with margin and fails to meet the other under the modeling assumptions adopted.

7. RESULTS

The framework of sections 2–6 was applied to the case-study bridge using the historical 1995 baseline TDPA of 2,772 vehicles per day per girder. A total of $N_{veh} = 1{,}011{,}780$ individual vehicle crossings were simulated for one calendar year, producing 1,002,583 rainflow stress cycles after the cycle-counting algorithm of section 3.1. Monte Carlo evaluation of the limit state used $N = 5 \times 10^5$ samples per point.

7.1 Stress range verification

Figure 4 shows the distribution of simulated stress ranges at or above 5 MPa. Cycles below this threshold, produced predominantly by passenger and light commercial vehicles, account for approximately 70% of the total count and are omitted for clarity. The remaining spectrum shows a heavy upper tail produced primarily by T3-S2-R4 trucks.

The simulated maximum stress range is 86.62 MPa, the 99th-percentile range is 61.18 MPa, and the 95th-percentile range is 32.08 MPa.

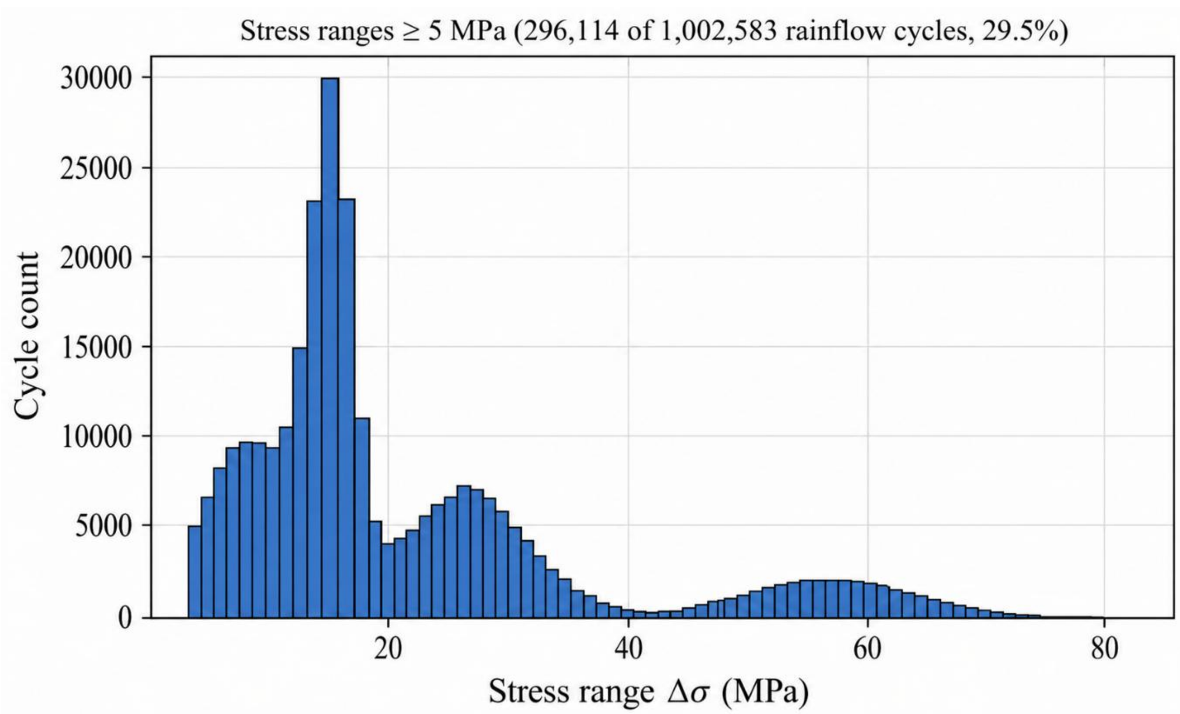

Figure 4. Distribution of simulated rainflow stress ranges at the analyzed cross-section. Showing cycles with Δσ ≥ 5 MPa. Cycles below this threshold, produced predominantly by passenger and light commercial vehicles, are omitted for clarity.

7.2 Per-year damage and nominal fatigue life.

Under the Eurocode bilinear S-N curve, the annual Miner damage at the reference daily average traffic volume is $D_{base} = 2.35 \times 10^{-3}$. Under the AASHTO single-slope curve, $D_{base} = 7.42 \times 10^{-5}$. The corresponding nominal years to $D = 1$ at constant traffic are 425.4 (Eurocode) and 13,469.9 (AASHTO).

The 30-fold ratio between the two values is a consequence of the position of the simulated stress spectrum relative to the constant-amplitude fatigue limit. For Detail Category 100, the CAFL is $\Delta\sigma_D = 73.7\ MPa$ and the cut-off is $\Delta\sigma_L = 40.5\ MPa$. Approximately 3.7% of the simulated cycles fall in the 40.5–73.7 MPa band, where the Eurocode $m_2 = 5$ branch continues to accumulate damage, but the AASHTO threshold model assigns zero contribution. Cycles above 73.7 MPa, where both formulations agree, constitute less than 0.1% of the total. The Eurocode formulation therefore captures damage from the small population of intermediate-amplitude cycles that the AASHTO formulation discards. This effect is examined in detail in the discussion.

7.3 Calibration at the central scenario.

For the central growth scenario $\alpha_{traffic} = 2.5\%/year$ and $T_{design} = 75\ years$, the calibrated load factors are summarized in Table 1.

Table 1. Calibrated load factor x_F at the central scenario ($\alpha_{traffic} = 2.5\%/yr$, $T_{design} = 75\ yr$).

S-N convention	$\boldsymbol{\beta_{target} = 1.0}$	$\boldsymbol{\beta_{target} = 3.0}$
Eurocode bilinear (EN 1993-1-9)	1.34	0.70
AASHTO single-slope	> 4.0*	> 4.0*

* Calibration at the upper bound of the search grid.

Under the Eurocode bilinear S-N convention, the calibration yields $x_F = 1.34$ at $\beta_{target} = 1.0$ and $x_F = 0.70$ at $\beta_{target} = 3.0$. Under the AASHTO single-slope convention, the calibration is unbounded by the upper limit of the search grid for both targets, indicating that the threshold model does not flag the case-study spectrum as fatigue-critical at any practical load factor. Figure 5 shows the variation in the reliability index given different load factor possibilities.

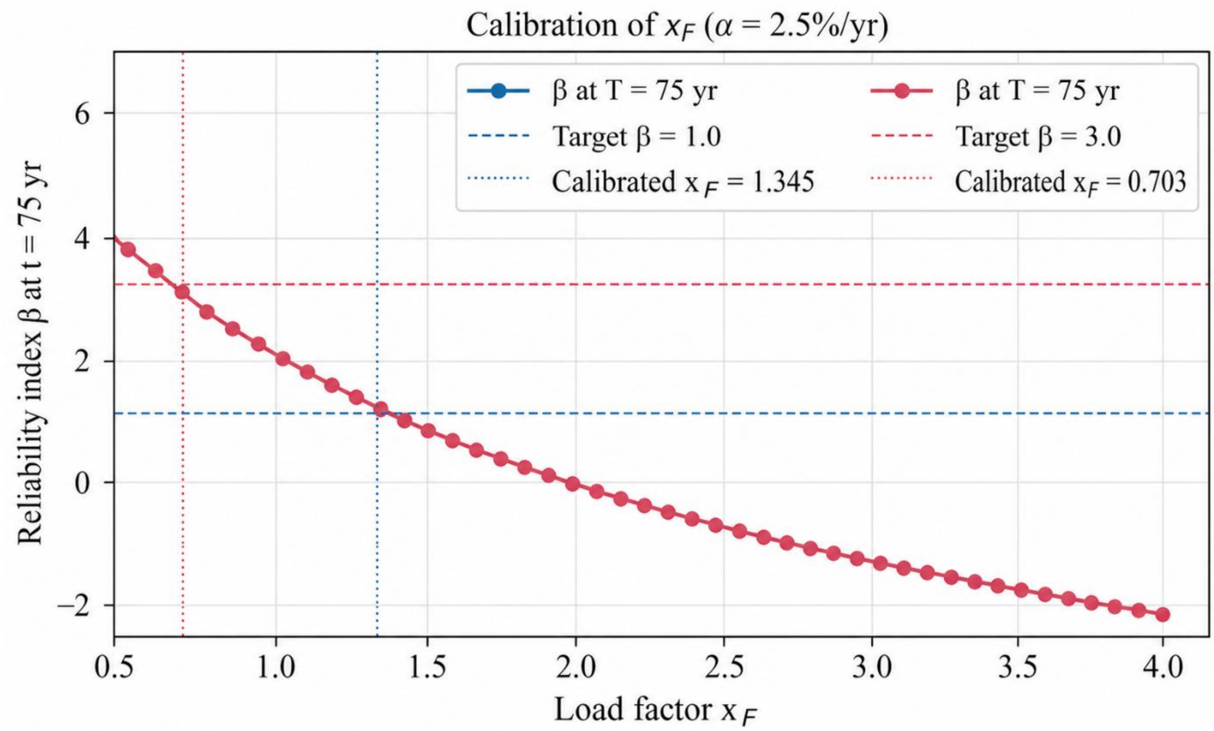

Figure 5. Calibration curve: reliability index $\beta(T_{design})$ as a function of the load factor x_F, under the Eurocode bilinear S-N convention and at the central growth scenario. Horizontal lines mark the two adopted reliability targets; vertical lines mark the corresponding calibrated values.

7.4 Sensitivity to traffic growth rate.

Holding the load factor fixed at the value calibrated for the central scenario at $\beta_{target} = 1.0$ ($x_F = 1.34$), the reliability index at the design horizon is evaluated across the full range of growth rates introduced in section 4. Figure 6 shows the resulting $\beta(t)$ trajectories. The reliability index at $T = 75$ years is approximately 3.68 for the lowest growth scenario ($\alpha_{traffic} = 0.5\%/yr$) and approximately −2.87 for the highest ($\alpha_{traffic} = 5\%/yr$), a span of 6.5 units in the reliability index from a tenfold variation in the assumed growth rate.

Within the limitations of the present modeling assumptions, this sensitivity emerged as the most influential numerical effect observed. Other examined input parameters, including the choice of S–N convention and the assumed detail category, were not observed to produce comparable changes in the reliability index at the design period.

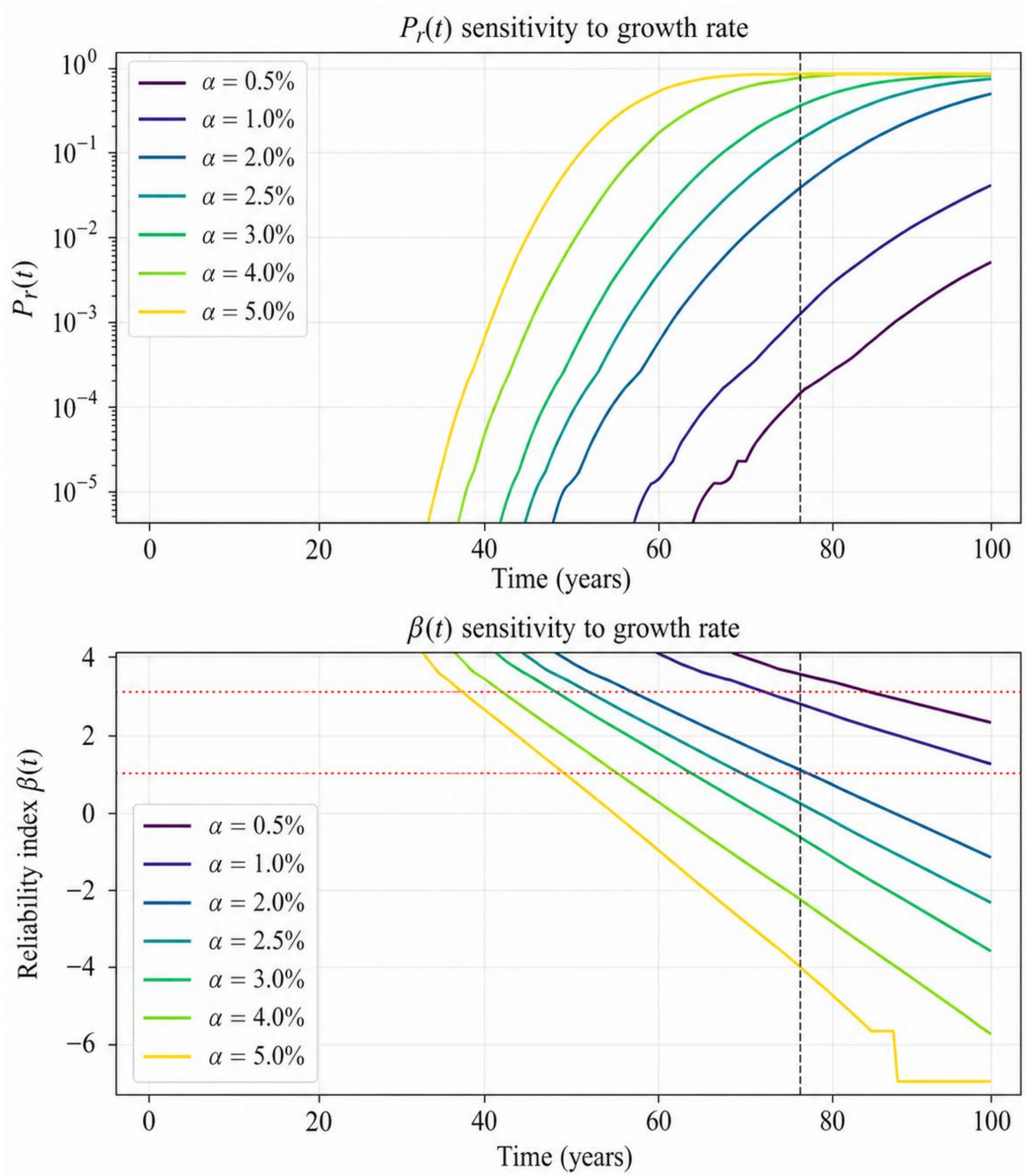

Figure 6. Sensitivity of the probability of failure $P_f(t)$ and the reliability index $\beta(t)$ to the assumed annual traffic growth rate $\alpha_{traffic}$, with the load factor fixed at the value calibrated for the central scenario ($x_F = 1.34$, $\beta_{target} = 1.0$).

8. DISCUSSION

8.1 Interpretation of calibrated factors.

Per the convention established in section 6.4, a calibrated value $x_F > 1$ indicates that the simulated loading produces a reliability index above the target and therefore could in principle accommodate x_F times more loading before reliability falls to the target. A calibrated value $x_F < 1$ indicates that the simulated loading produces reliability below the target, with the factor representing the fraction of simulated loading at which the target would be met.

For the central growth scenario at $\beta_{target} = 1.0$, the Eurocode calibration yields $x_F = 1.34$, indicating the bridge could in principle carry 34% more loading before its reliability falls to the AASHTO-aligned target. The same scenario at $\beta_{target} = 3.0$ yields $x_F = 0.70$, indicating the simulated loading would need to be reduced by 30% to bring reliability to the JCSS-aligned target. The unfactored loading at $x_F = 1$ therefore produces a reliability index between the two targets: above $\beta = 1.0$ (the bridge meets the AASHTO-aligned target with margin) but below $\beta = 3.0$ (the bridge falls short of the Eurocode-aligned target).

8.2 Mexican legal vehicles compared to design vehicles.

The Mexican operating environment has gross vehicle weights substantially higher than those of the design vehicles used to calibrate either AASHTO or Eurocode fatigue load models. The AASHTO HS20-44 design vehicle has a gross weight of approximately 325 kN (3 axles); the heaviest legal Mexican configuration, T3-S2-R4, has a maximum gross weight of 740.4 kN (75.5 t, 9 axles) (DOF, 2017), approximately 2.28 times the AASHTO design vehicle. García-Soto et al. (2015) report a probabilistic Mexican design truck model with mean gross weight of approximately 652 kN, intermediate between the two. Beyond the legal limits, the IMT field campaign at the case-study station shows substantial in-service overloading: 24% of weighed T3-S2-R4 vehicles exceeded the legal 740.4 kN (75.5 t) limit, and the maximum observed gross vehicle weight reached 92.4 t (1.22 times the legal limit). Compounded, the heaviest single-vehicle observation in the IMT campaign exceeds the AASHTO HS20-44 design loading by a factor of approximately 2.79. The disconnect between the loadings against which the codes were calibrated and those actually observed on Mexican infrastructure is itself a strong motivation for explicit, Mexico-specific calibration of fatigue load factors. Avendaño et al. (2013), working from SCT (2001) overloading survey data, proposed a design vehicle with a gross vehicle weight of 958.2 kN representing the upper-bound mean of overloaded T3-S2-R4 vehicles observed at that time.

8.3 Eurocode–AASHTO divergence.

The difference between the Eurocode and AASHTO computed annual damages merits further discussion. The two formulations are mathematically identical above the constant-amplitude fatigue limit ($\Delta\sigma \geq \Delta\sigma_D = 73.7\ MPa$ for Detail Category 100), where both adopt $m = 3$ and the same intercept. They differ only in the sub-CAFL regime: the Eurocode bilinear curve continues to accumulate damage along an $m_2 = 5$ branch down to a cut-off at $\Delta\sigma_L = 40.5\ MPa$, while the AASHTO single-slope curve assigns zero damage to all cycles below the threshold.

For the case-study spectrum, the upper tail of stress ranges sits predominantly in this 40.5–73.7 MPa band: approximately 3.7% of cycles fall there, but their contribution under the Eurocode $m_2 = 5$ branch dominates the total damage because cycles at $\Delta\sigma > 73.7\ MPa$ are rare (less than 0.1% of the total). The AASHTO formulation may therefore neglect what appears to be, for this spectrum, the principal damaging contribution. The 30-fold ratio is a consequence of the position of the spectrum's upper tail relative to the CAFL, a property of the bridge and its loading. Under a heavier-loaded bridge with a substantial fraction of cycles above 73.7 MPa, the two formulations would converge.

The Eurocode bilinear formulation is preferred as the primary calibration tool. AASHTO results are reported alongside Eurocode for comparison.

8.4 Growth rate as a potentially dominant source of uncertainty.

Across the full sensitivity range examined, the assumed annual traffic growth rate produces a shift in the reliability index at the design horizon of 6.5 units. Under fixed load factor, varying the growth rate by a factor of ten, from 0.5%/year to 5%/year, shifts $\beta(T = 75)$ from approximately 3.7 to approximately −2.8.

By comparison, alternative assumptions on the modeling-uncertainty coefficient COV_e in the range 0.10–0.20 produce shifts in the calibrated factor of less than 5%, and a one-category change in detail category (Cat 80 versus Cat 125) produces shifts of approximately 30%. Growth rate may therefore be the dominant input uncertainty for the calibration over a 75-year period. This identifies a possible gap in current code practice, since design code fatigue load factors are not formulated via the local growth rate.

8.5 Continued service of the case-study bridge.

The case-study bridge has been in service since 1995 and is reported as operational. The nominal years-to-failure under the Eurocode formulation (425 years at constant traffic; on the order of 100 years under the central growth scenario) is consistent with this empirical observation rather than at odds with it: under the modeling assumptions adopted, fatigue is a meaningful design check at the case-study site but is not the controlling failure mode at present-day loadings. The contribution of the calibration is to establish how this margin evolves under projected growth, not to predict imminent failure of the existing structure.

8.6 Limitations.

The calibration reported above is conditional on several modeling choices that merit explicit acknowledgment. Firstly, the calibration is based on a single bridge and a single weigh-in-motion station. National-scale calibration of a fatigue load factor along the lines of NCHRP Report 368 (Nowak, 1999) would require a representative population of bridges, multiple WIM sites, and a structured weighting of bridge types and traffic environments. Therefore, the factors reported here should be read as case-specific demonstrations of the calibration methodology rather than as generalized proposals for code adoption.

Likewise, the case-study bridge is a five-span continuous composite structure. The analysis idealizes a single steel girder as simply supported over a span of 76.5 m and applies a constant correction factor $k = 0.7$ to the simulated midspan moment to approximately account for continuous-span behavior, following Johnson et al. (2020). Likewise, the composite action between the steel girder and the concrete deck is acknowledged but not modeled explicitly. Composite action would shift the neutral axis upward and reduce the stress. Finally, the structural cross-section properties themselves ($I = 0.1089\ m^4$, $A = 0.1637\ m^2$, depth 2.0 m) are scaled estimates from Meneses Rojas (2026), who states that the geometry is an approximation.

Regarding the structural idealization, the analysis treats the vehicle-bridge interaction as quasi-static and does not apply a dynamic load factor, for the reasons set out in section 2.4. A refinement of the present framework would incorporate a span-dependent and speed-dependent dynamic amplification rather than a single uniform factor, ideally calibrated against field measurements of the case-study structure. This would allow the dynamic contribution to be represented in the stress spectrum itself rather than as a uniform scaling of the moment history.

The configuration of Puente Calapa (single lane per direction, two girders) allows the case study analysis to sidestep explicit modeling of simultaneous multi-vehicle presence, as discussed in section 2.4. This simplification would not apply to multi-lane bridges where several heavy vehicles can share a girder's tributary area at highway speed. Therefore, extending the calibration to such configurations is a possible direction for future work. Likewise, strain measurements at the case-study structure would provide independent validation of the simulated stress spectrum.

Finally, the fatigue detail at the analyzed cross-section is assumed to correspond to EN 1993-1-9 Detail Category 100 (continuous longitudinal fillet weld between web and bottom flange of a built-up plate girder). A different controlling detail would shift the CAFL and modify the simulated stress spectrum. As discussed in section 8.3, the ratio between Eurocode and AASHTO computed damage is sensitive to this positioning; the calibrated load factor is correspondingly sensitive to the assumed detail category.

9. CONCLUSIONS

This study presented a reliability-based calibration of the fatigue load factor for a Mexican steel bridge in which the annual traffic growth rate was treated as an explicit input to the calibration rather than embedded implicitly in the resulting factor. For the central growth scenario ($\alpha_{traffic} = 2.5\%/year$, $T_{design} = 75\ years$), the Eurocode bilinear S-N convention yields calibrated load factors of $x_F = 1.34$ at $\beta_{target} = 1.0$ and $x_F = 0.70$ at $\beta_{target} = 3.0$, indicating that the unfactored loading produces a reliability between the two adopted targets. Across the growth range examined, the assumed annual growth rate shifted the reliability index at the design horizon by approximately 6.5 units, a larger effect than that observed for any other input parameter examined in the present analysis. Within the limitations of the single-bridge case study, this suggests that explicit formulation of fatigue load factors by the local traffic growth rate is a possible direction for future code calibration work in environments where heavy-traffic growth differs substantially from the assumptions implicit in existing factors.

10. REFERENCES

AASHTO. (2024), *LRFD Bridge Design Specifications*, 10th Edition. American Association of State Highway and Transportation Officials, Washington, DC. ISBN: 978-1-56051-828-0

ASTM International. (2017), *ASTM E1049-85 Standard Practices for Cycle Counting in Fatigue Analysis*. https://doi.org/10.1520/E1049-85R17

Avendaño, A., Gómez-Soberón, M., Perea, T. (2013), *Evaluación elástica simplificada por fatiga de un puente de acero tipo ortotrópico bajo cargas móviles típicas de México*. XIX Congreso Nacional de Ingeniería Sísmica, Boca del Río, Veracruz, México. Sociedad Mexicana de Ingeniería Sísmica.

Berwick, B. (2012), *Calibrating the steel-members fatigue limit states of the AASHTO LRFD bridge design specifications*, PhD thesis, University of Delaware. Recuperado en abril de 2026 de http://udspace.udel.edu/handle/19716/12642

Bowman, M. D., Fu, G., Zhou, Y. E., Connor, R. J., Godbole, A. A. (2012), *Fatigue evaluation of steel bridges (NCHRP Report 721).* Transportation Research Board, Washington, D.C. ISBN: 978-0-309-25826-5. https://doi.org/10.17226/22774

CEN (European Committee for Standardization). (2005), *Eurocode 3: Design of steel structures — Part 1-9: Fatigue (EN 1993-1-9).* CEN, Brussels.

CEN (European Committee for Standardization). (2006), *Eurocode 3: Design of steel structures — Part 2: Steel bridges (EN 1993-2).* CEN, Brussels.

D'Angelo, L., Nussbaumer, A. (2017), *New framework for calibration of partial safety factors for fatigue design.* Journal of Constructional Steel Research, 139:466–472. https://doi.org/10.1016/J.JCSR.2017.10.006

DOF (Diario Oficial de la Federación). (2017), *NOM-012-SCT-2-2017, Sobre el peso y dimensiones máximas con los que pueden circular los vehículos de autotransporte que transitan en las vías generales de comunicación de jurisdicción federal.* Recuperado en junio de 2026 de https://www.dof.gob.mx/nota_detalle_popup.php?codigo=5508944

García-Soto, A. D., Hernández-Martínez, A., Valdés-Vázquez, J. G. (2015), Probabilistic assessment of a design truck model and live load factor from weigh-in-motion data for Mexican Highway bridge design. Canadian Journal of Civil Engineering, 42(11). https://doi.org/10.1139/cjce-2015-0216

Google Earth. (2026, agosto 5), [*Imagen satelital de 18°09'46.73"N 97°15'35.07"W*]. Recuperado de https://earth.google.com/

IMT (Instituto Mexicano del Transporte). (2016), *Estudio de Origen–Destino y Peso, Estación PC Tehuacán, Carretera Cuacnopalan–Oaxaca (Cuota), km 40+850. Estudio Estadístico de Campo del Autotransporte Nacional (EECAN)*, Coordinación de Seguridad y Operación del Transporte. Campaña del 31 mayo hasta 03 junio 2016. Archivo: 357PcTehuacan.DBF. Recuperado en mayo de 2026 de https://www.gob.mx/imt/articulos/estudio-estadistico-de-campo-del-autotransporte-nacional

JCSS (Joint Committee on Structural Safety). (2011), *JCSS Probabilistic Model Code, Part 3.12: Fatigue Models for Metallic Structures.* Recuperado en junio 2026 de https://www.jcss-lc.org/publications/jcsspmc/JCSS-3-12-Fatigue.pdf

Johnson, C., Rakoczy, A., Otter, D., Dick, S. (2020), *Comparison of continuous spans versus simply supported spans* (Technology Digest TD20-024). Transportation Technology Center, Inc., Pueblo, CO. Recuperado en mayo de 2026 de https://www.mxvrail.com/technology-digest/comparison-of-continuous-spans-versus-simply-support-spans/

Kwon, K., Frangopol, D. M. (2010), *Bridge fatigue reliability assessment using probability density functions of equivalent stress range based on field monitoring data.* International Journal of Fatigue, 32(8):1221–1232. https://doi.org/10.1016/j.ijfatigue.2010.01.002

Matsuishi, M., Endo, T. (1968), *Fatigue of metals subjected to varying stress.* Proceedings of the Kyushu District Meeting, Japan Society of Mechanical Engineers, Fukuoka, Japan. Recuperado en mayo de 2026 de https://www.semanticscholar.org/paper/Fatigue-of-metals-subjected-to-varying-stress-Matsuichi-Endo/467c88ec1feaa61400ab05fbe8b9f69046e59260

Meneses Rojas, L. A. (2026), *Metodología de estimación de confiabilidad de fatiga por daño acumulado en puentes vehiculares bajo carga cíclica*, MSc thesis, Benemérita Universidad Autónoma de Puebla.

Miner, M. A. (1945), *Cumulative Damage in Fatigue*. Journal of Applied Mechanics, 12(3):A159–A164. https://doi.org/10.1115/1.4009458

Moses, F., Schilling, C. G., Raju, K. S. (1987), *Fatigue evaluation procedures for steel bridges.* NCHRP Report 299. Recuperado en abril de 2026 de https://trid.trb.org/View/282602, ISSN: 0077-5614

Nowak, A. S. (1999), *Calibration of LRFD Bridge Design Code (NCHRP Report 368)* Transportation Research Board, Washington, DC. ISSN 0077-5614

SCT (Secretaría de Infraestructura, Comunicaciones y Transportes). (s.f.), *Datos Viales.* Recuperado en abril de 2026 de https://micrs.sct.gob.mx/infraestructura/direccion-general-de-servicios-tecnicos/datos-viales/

Sørensen, J. D. (2012), *Reliability-based calibration of fatigue safety factors for offshore wind turbines.* International Journal of Offshore and Polar Engineering, 22(3):234–241.

Suarez, J. (2025), *Puente Calapa, una peligrosa ruta entre Puebla y Oaxaca—El Sol de Puebla.* El Sol de Puebla. Recuperado en agosto de 2026 de https://oem.com.mx/elsoldepuebla/local/puente-calapa-una-peligrosa-ruta-entre-puebla-y-oaxaca-23407734

TRB (Transportation Research Board and National Academies of Sciences, Engineering, and Medicine). (2014), *Bridges for Service Life Beyond 100 Years: Service Limit State Design.* The National Academies Press, Washington, DC. https://doi.org/10.17226/22441

Wirsching, P. H. (1984), *Fatigue Reliability for Offshore Structures.* Journal of Structural Engineering, 110(10), 2340–2356. https://doi.org/10.1061/(ASCE)0733-9445(1984)110:10(2340)

Zhang, M., Wang, X., Li, Y. (2024), *Fatigue Reliability Assessment of Bridges Under Heavy Traffic Loading Scenario*. Infrastructures, 9(12):238. https://doi.org/10.3390/infrastructures9120238